NATURAL CONVECTION IN SQUARE ENCLOSURES DIFFERENTIALLY HEATED AT SIDES USING ALUMINA-WATER NANOFLUIDS WITH TEMPERATURE-DEPENDENT PHYSICAL PROPERTIES

by

Marta CIANFRINI, Massimo CORCIONE*, and Alessandro QUINTINO

Deparment of Aereonautical, Electrical and Energetic Engineering,
Sapienza University of Rome, Italy

Original scientific paper
DOI: 10.2298/TSCI120328111C

Laminar natural convection of $Al_2O_3 + H_2O$ nanofluids inside square cavities differentially heated at sides is studied numerically. A computational code based on the SIMPLE-C algorithm is used for the solution of the system of the mass, momentum, and energy transfer governing equations. Assuming that the nanofluid behaves like a single-phase fluid, these equations are the same as those valid for a pure fluid, provided that the thermophysical properties appearing in them are the nanofluid effective properties. The thermal conductivity and dynamic viscosity of the nanofluid are calculated by means of a couple of empirical equations based on a wide variety of experimental data reported in the literature. The other effective properties are evaluated by the conventional mixing theory. Simulations are performed for different values of the nanoparticle volume fraction in the range 0-0.06, the diameter of the suspended nanoparticles in the range 25-100 nm, the temperature of the cooled sidewall in the range 293-313 K, the temperature of the heated sidewall in the range 298-343 K, and the Rayleigh number of the base fluid in the range 10^3-10^7. All computations are executed in the hypothesis of temperature-dependent effective properties. The main result obtained is the existence of an optimal particle loading for maximum heat transfer, that is found to increase as the size of the suspended nanoparticles is decreased, and the nanofluid average temperature is increased.

Key words: *nanofluid, temperature-dependent physical properties, natural convection, side-heated enclosure, numerical analysis*

Introduction

Buoyancy-induced heat transfer in enclosures differentially heated at sides is of great practical importance in a multitude of engineering applications, such as the cooling of electronic assemblies and the collection of solar energy, to name a few. Actually, thermal designers often prefer to avoid the use of mechanical equipment for the fluid circulation, especially when a small power consumption, a negligible operating noise, and a high reliability of the system, are main concerns. However, the intrinsic low performance of natural convection, in comparison with equivalent or similar forced convection situations, represents a substantial restriction to heat transfer. A possible solution to mitigate the problem could be the replacement of traditional heat transfer fluids (such as water, ethylene glycol and mineral oils) with nanofluids, *i. e.* liquid suspensions of nanosized solid particles, whose effective thermal con-

* Corresponding author; e-mail: massimo.corcione@uniroma1.it

ductivity is known to be higher than that of the corresponding pure base liquid. On the other hand, a survey of the articles dealing with natural convection of nanofluids in vertical cavities reveals that the question if the use of nanoparticle suspensions is really advantageous with respect to pure liquids seems to be not yet answered. In fact, according to some authors, the addition of nanoparticles to a base liquid implies a more or less remarkable enhancement of the heat transfer rate [1-7], whilst, according to others, a deterioration may occur [8-10].

The reason for such conflicting results can be explained by considering that the heat transfer performance of nanofluids in natural convection flows is a strict consequence of the two opposite effects arising from the increase of the effective thermal conductivity and dynamic viscosity occurring as the volume fraction of the suspended nanoparticles is augmented. In other words, the dispersion of a given concentration of nanoparticles into a base liquid can bring to either an enhancement or a degradation of the heat transfer performance, depending on whether the increased thermal conductivity effect is larger or smaller than the increased viscosity effect.

Now, the majority of the studies available in the literature are numerical studies based on the common assumption that nanofluids behave more like single-phase fluids rather than like conventional solid-liquid mixtures. This means that the mass, momentum, and energy transfer governing equations for pure fluids can be directly extended to nanoparticle suspensions, provided that the thermophysical properties appearing in them are the nanofluid effective properties. Of course, the use of robust theoretical models or empirical equations, capable to predict the nanofluid effective properties as more accurately as possible, is crucial for obtaining realistic data. Unfortunately, most of the studies cited above miss this requirement, for one reason or another, thus leading to unreliable results.

Typically, erroneous results derived from the calculation of the effective thermal conductivity and dynamic viscosity by the Maxwell-Garnett model [11] and the Brinkman equation [12], which belong to the category of the traditional mean-field theories, originally developed for composites and mixtures with micro-sized and milli-sized inclusions. In fact, the Maxwell-Garnett model, and the other traditional models commonly used to predict the effective thermal conductivity (such as the Hamilton-Crosser model [13], and the Bruggemann model [14]), appear to be suitable to this end when the nanofluid is at ambient temperature, *e. g*. Eapen *et al.* [15], and Buongiorno *et al.* [16], but tend to fail dramatically when the temperature of the suspension is one or some tens degrees higher than 20-25 °C, *e. g.* shown experimentally by Das *et al.* [17], Li and Peterson [18], and Yu *et al.* [19]. In its turn, the Brinkman equation is known to underestimate the actual values of the dynamic viscosity of nanofluids, with a degree of underestimation that increases significantly as the nanoparticle diameter decreases and the nanoparticle concentration increases, *e. g.* demonstrated by Chen *et al.* [20, 21], and Chevalier *et al.* [22]. Same considerations apply to the Einstein equation [23, 24], sometimes used instead of the Brinkman equation to evaluate the effective dynamic viscosity. In other cases, misleading conclusions were achieved because the nanofluid effective properties were evaluated by either partly inconsistent semi-empirical models, or correlations based on experimental data whose values are inexplicably in contrast with the main body of the literature results, or equations whose validity was restricted to situations very different from those investigated.

As far as the experimental studies are concerned, the first of them was performed in 2003 by Putra *et al.* [25], who used a horizontal cylindrical vessel differentially heated at ends, containing Al_2O_3 (d_p = 131.2 nm) + H_2O, or CuO (d_p = 87.3 nm) + H_2O with volume fractions of 1% and 4%. The average Nusselt number of the enclosure was found to decrease

with increasing the nanoparticle volume fraction. The common interpretation of this result is that a heat transfer deterioration occurred with increasing the concentration of the suspended nanoparticles. Indeed, owing to the increase of the effective thermal conductivity, k, a decrease of the Nusselt number does not necessarily mean that the heat transfer rate decreases. It may occur that for a given nanoparticle volume fraction, φ, the coefficient of convection of the nanofluid, h, is higher than that of the pure base liquid, h_f (thus meaning that the addition of nanoparticles to the base liquid enhances the thermal performance of the enclosure), but if $(\partial h/\partial k) < 0$ the average Nusselt number of the nanofluid is smaller than that of the pure base liquid. This is exactly the case of the Nusselt numbers reported by Putra, *et al.* for $\varphi = 0.01$. Indeed, if these data are properly rearranged in order to obtain the values of the ratio h/h_f, a heat transfer enhancement may be clearly observed. *Vice versa*, at $\varphi = 0.04$ a slight heat transfer degradation occurred for both nanofluids investigated, thus implying the existence of an optimal particle loading.

A smooth optimal particle loading for maximum heat transfer across a cavity filled with Al_2O_3 (d_p = 27 nm) + H_2O was later discovered experimentally by Nnanna [26], who explained its existence as the consequence of an excessive increase in viscosity that occurred above a certain nanoparticle concentration. Such optimal nanoparticle concentration, whose existence can also be inferred from an attentive analysis of the experimental data recently published by Ho *et al.* [27] for a square enclosure filled with Al_2O_3 (d_p = 33 nm) + H_2O, was calculated by Corcione [28] in a first-approach, theoretical work. In particular, the heat transfer enhancement and the optimal volume fraction were found to increase as the nanoparticle diameter was decreased and both the nanofluid average temperature and the aspect ratio of the enclosure were increased.

Framed in this general background, the aim of the present paper is to undertake a comprehensive numerical study on natural convection in a differentially heated vertical enclosure filled with a water suspension of alumina nanoparticles having temperature-dependent effective properties, with the primary scope to investigate the main features of heat transfer and fluid flow, and determine accurate correlations for predicting the optimal particle loading and the amount of heat transferred across the cavity.

Mathematical formulation

A square enclosure of width W containing an alumina-water nanofluid is differentially heated at the vertical walls, that are kept at uniform temperatures T_h and T_c, whilst the top and bottom walls are perfectly insulated, as depicted in fig. 1. A zero surface emissivity is assumed for the confining walls, which physically corresponds to perfectly polished surfaces, thus implying that the present situation involves pure natural convection, owing to the absence of any contribution by radiation.

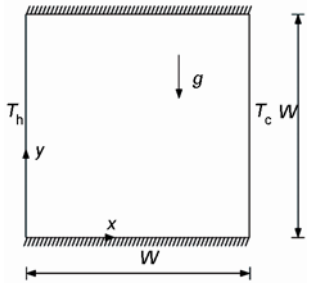

Figure 1. Sketch of the geometry and co-ordinate system

According to the approach typically used in most studies performed on this same subject, the nanofluid is handled as a single-phase fluid. In fact, since the suspended nanoparticles have usually small size and concentration, the hypothesis of a solid-liquid mixture statistically homogeneous and isotropic can reasonably be advanced. This means that, under the further assumptions that the nanoparticles and base liquid are in local thermal equilibrium, and no slip motion occurs between the solid and liquid phases, to all intents and purposes the nanofluid can be treated as a pure fluid. Thus, the equations that govern

the flow and heat transfer valid for pure fluids can be directly extended to the nanoparticle suspension, provided that the thermophysical properties appearing in them are the nanofluid effective properties. Such a formulation finds experimental confirmation in the study performed by Chang *et al.* [29], who demonstrated that the same Nusselt-Rayleigh correlation valid for layers of pure water is applicable with good approximation to nanofluid layers consisting of Al_2O_3 (d_p = 250 nm) + H_2O if both Nusselt and Rayleigh numbers are calculated using the thermophysical properties of the suspension. Same type of experimetal results were obtained for forced convection flows by Williams *et al.* [30], Sommers and Yerkes [31], and Rea *et al.* [32]. Additionally, the nanofluid is treated as a Newtonian fluid, which was demonstrated *e. g.* by Putra *et al.* [25, 33], Prasher *et al.* [34], He *et al.* [35], Chen *et al.* [20, 21], and Chevalier *et al.* [22].

Therefore, assuming that the flow is steady, 2-D, laminar, and incompressible, with negligible viscous dissipation and pressure work, and that the nanofluid effective properties depend on temperature, the conservation equations of mass, momentum, and energy reduce to, *e. g.* Kays *et al.* [36]:

$$\frac{\partial(\rho u)}{\partial x}+\frac{\partial(\rho v)}{\partial y}=0 \tag{1}$$

$$\rho\left(u\frac{\partial u}{\partial x}+v\frac{\partial u}{\partial y}\right)=-\frac{\partial p}{\partial x}+\frac{\partial}{\partial x}\left[2\mu\frac{\partial u}{\partial x}-\frac{2}{3}\mu\left(\frac{\partial u}{\partial x}+\frac{\partial v}{\partial y}\right)\right]+\frac{\partial}{\partial y}\left[\mu\left(\frac{\partial u}{\partial y}+\frac{\partial v}{\partial x}\right)\right] \tag{2}$$

$$\rho\left(u\frac{\partial v}{\partial x}+v\frac{\partial v}{\partial y}\right)=-\frac{\partial p}{\partial y}+\frac{\partial}{\partial y}\left[2\mu\frac{\partial v}{\partial y}-\frac{2}{3}\mu\left(\frac{\partial u}{\partial x}+\frac{\partial v}{\partial y}\right)\right]+\frac{\partial}{\partial x}\left[\mu\left(\frac{\partial u}{\partial y}+\frac{\partial v}{\partial x}\right)\right]-\rho g \tag{3}$$

$$\rho u\frac{\partial(cT)}{\partial x}+\rho v\frac{\partial(cT)}{\partial y}=\frac{\partial}{\partial x}\left(k\frac{\partial T}{\partial x}\right)+\frac{\partial}{\partial y}\left(k\frac{\partial T}{\partial y}\right) \tag{4}$$

where x and y are the horizontal and vertical Cartesian co-ordinates, u and v – the x-wise, and y-wise velocity components, p is the pressure, T – the temperature, g – the acceleration of gravity, ρ – the effective mass density, μ – the effective dynamic viscosity, c – the effective specific heat at constant pressure, and k – the effective thermal conductivity.

Once the following dimensionless variables are introduced:

$$X=\frac{x}{W},\quad Y=\frac{y}{W} \tag{5}$$

$$U=\frac{u}{\frac{\mu_r}{\rho_r W}},\quad V=\frac{v}{\frac{\mu_r}{\rho_r W}},\quad P=\frac{p-p_r}{\frac{\mu_r^2}{\rho_r W^2}},\quad \theta=\frac{T-T_r}{T_h-T_c} \tag{6}$$

$$\rho^*=\frac{\rho}{\rho_r},\quad \mu^*=\frac{\mu}{\mu_r},\quad c^*=\frac{c}{c_r},\quad k^*=\frac{k}{k_r} \tag{7}$$

the governing equations become:

$$\frac{\partial(\rho^* U)}{\partial X}+\frac{\partial(\rho^* V)}{\partial Y}=0 \tag{8}$$

$$\rho^*\left(U\frac{\partial U}{\partial X}+V\frac{\partial U}{\partial Y}\right)=-\frac{\partial P}{\partial X}+\frac{\partial}{\partial X}\left[2\mu^*\frac{\partial U}{\partial X}-\frac{2}{3}\mu^*\left(\frac{\partial U}{\partial X}+\frac{\partial V}{\partial Y}\right)\right]+\frac{\partial}{\partial Y}\left[\mu^*\left(\frac{\partial U}{\partial Y}+\frac{\partial V}{\partial X}\right)\right] \quad (9)$$

$$\rho^*\left(U\frac{\partial V}{\partial X}+V\frac{\partial V}{\partial Y}\right)=-\frac{\partial P}{\partial Y}+\frac{\partial}{\partial Y}\left[2\mu^*\frac{\partial V}{\partial Y}-\frac{2}{3}\mu^*\left(\frac{\partial U}{\partial X}+\frac{\partial V}{\partial Y}\right)\right]+$$
$$+\frac{\partial}{\partial X}\left[\mu^*\left(\frac{\partial U}{\partial Y}+\frac{\partial V}{\partial X}\right)\right]+\frac{\mathrm{Ra}}{\mathrm{Pr}}\frac{\rho_\mathrm{r}-\rho}{\rho_\mathrm{c}-\rho_\mathrm{h}} \quad (10)$$

$$\rho^*U\frac{\partial(c^*\theta)}{\partial X}+\rho^*V\frac{\partial(c^*\theta)}{\partial Y}=\frac{1}{\mathrm{Pr}}\left[\frac{\partial}{\partial X}\left(k^*\frac{\partial\theta}{\partial X}\right)+\frac{\partial}{\partial Y}\left(k^*\frac{\partial\theta}{\partial Y}\right)\right] \quad (11)$$

where Ra and Pr are the effective Rayleigh and Prandtl numbers defined as:

$$\mathrm{Ra}=\frac{\rho_\mathrm{r}c_\mathrm{r}\mathrm{g}(\rho_\mathrm{c}-\rho_\mathrm{h})W^3}{k_\mathrm{r}\mu_\mathrm{r}},\quad \mathrm{Pr}=\frac{c_\mathrm{r}\mu_\mathrm{r}}{k_\mathrm{r}} \quad (12)$$

In the preceding equations the effective properties with subscript "r" are calculated at the reference temperature T_r, that is conventionally set equal to the temperature T_c of the cooled sidewall of the enclosure, whereas ρ_h, and ρ_c are the values of the effective mass density calculated at temperatures T_h and T_c, respectively.

Fixed $T_\mathrm{r} = T_\mathrm{c}$, the thermal boundary conditions expressed in the proper dimensionless form are:

– $\theta = 1$ at the heated sidewall,
– $\theta = 0$ at the cooled sidewall, and
– $\partial\theta/\partial Y = 0$ at the adiabatic top and bottom walls.

As regards the velocity boundary conditions, the no-slip condition $U = V = 0$ is assumed along the four confining walls.

Obviously, at any location inside the enclosure the effective physical properties ρ, μ, c, and k must be calculated at the location own temperature $T = T_\mathrm{c} + \theta(T_\mathrm{h} - T_\mathrm{c})$. This means that, although the governing equations are expressed in dimensionless form (which seems convenient for comparison purposes), the dependence of the effective physical properties on temperature requires that the set of independent variables must include both dimensional temperatures of the heated and cooled sidewalls, T_h and T_c, respectively.

The effective thermal conductivity and dynamic viscosity, k and μ, respectively, are calculated through the following empirical correlations obtained by Corcione [37] on the basis of a wide variety of experimental data available in the literature:

$$\frac{k}{k_\mathrm{f}}=1+4.4\,\mathrm{Re}^{0.4}\,\mathrm{Pr}_\mathrm{f}^{0.66}\left(\frac{T}{T_\mathrm{fr}}\right)^{10}\left(\frac{k_\mathrm{s}}{k_\mathrm{f}}\right)^{0.03}\varphi^{0.66} \quad (13)$$

$$\frac{\mu}{\mu_\mathrm{f}}=\frac{1}{1-34.87\left(\dfrac{d_\mathrm{p}}{d_\mathrm{f}}\right)^{-0.3}\varphi^{1.03}} \quad (14)$$

where k_f is the thermal conductivity of the base fluid, Re – the nanoparticle Reynolds number, Pr_f – the Prandtl number of the base fluid, T – the nanofluid temperature, T_fr – the freezing

point of the base fluid, k_s – the thermal conductivity of the solid nanoparticles, μ_f – the dynamic viscosity of the base fluid, d_f – the equivalent diameter of a base fluid molecule, and φ – the nanoparticle volume fraction. The standard deviations of error of eqs. (13) and (14) are 1.86% and 1.84%, respectively.

The Reynolds number of the suspended nanoparticles is defined as $(\rho_f u_B d_p)/\mu_f$, where ρ_f is the mass density of the base fluid, and u_B – the nanoparticle Brownian velocity. u_B is defined as the ratio between d_p and the time required to cover such a distance $\tau_D = (d_p)^2/6D$, where $D = (k_b T)/(3\pi\mu_f d_p)$ is the Einstein diffusion coefficient [38]. Accordingly, the following relation holds:

$$\mathrm{Re} = \frac{2\rho_f k_b T}{\pi \mu_f^2 d_p} \tag{15}$$

wherein $k_b = 1.38066 \cdot 10^{-23}$ J/K is the Boltzmann constant.

The equivalent diameter of a base fluid molecule is calculated at the reference temperature $T_0 = 293$ K on the basis of the relation $M = \rho_{f0} V_m \mathrm{N}$, where M, ρ_{f0}, and V_m are the molar mass, the mass density at T_0, and the molecular volume of the base fluid, whilst $\mathrm{N} = 6.022 \cdot 10^{23}$ mol^{-1} is the Avogadro number. If we express V_m as $(4/3)\pi(d_f/2)^3$, we obtain:

$$d_f = \left(\frac{6M}{\mathrm{N}\pi\rho_{f0}} \right)^{1/3} \tag{16}$$

The effective mass density of the nanofluid, ρ, is given by [39]:

$$\rho = (1-\varphi)\rho_f + \varphi\rho_s \tag{17}$$

where ρ_f and ρ_s are the mass densities of the base fluid and the solid nanoparticles, respectively.

Finally, the heat capacity at constant pressure per unit volume of the nanofluid, ρc, is calculated as [40]:

$$\rho c = (1-\varphi)(\rho c)_f + \varphi(\rho c)_s \tag{18}$$

where $(\rho c)_f$ and $(\rho c)_s$ are the heat capacities at constant pressure per unit volume of the base fluid and the solid nanoparticles, respectively. Hence, the effective specific heat at constant pressure of the nanofluid, c, is given by:

$$c = \frac{(1-\varphi)(\rho c)_f + \varphi(\rho c)_s}{(1-\varphi)\rho_f + \varphi\rho_s} \tag{19}$$

Once the effective physical properties are properly evaluated, the effective Rayleigh and Prandtl numbers that must be used in eqs. (10) and (11), can be expressed as functions of the Rayleigh and Prandtl numbers of the base fluid, Ra_f and Pr_f, by the following relations:

$$\mathrm{Ra} = \mathrm{Ra}_f \frac{\left(\frac{\rho}{\rho_f}\right)_r \left(\frac{c}{c_f}\right)_r}{\left(\frac{k}{k_f}\right)_r \left(\frac{\mu}{\mu_f}\right)_r} \frac{\rho_c - \rho_h}{(\rho_f)_c - (\rho_f)_h}, \quad \mathrm{Pr} = \mathrm{Pr}_f \frac{\left(\frac{c}{c_f}\right)_r \left(\frac{\mu}{\mu_f}\right)_r}{\left(\frac{k}{k_f}\right)_r} \tag{20}$$

where $(\rho_f)_h$ and $(\rho_f)_c$ are the values of the mass density of the base fluid calculated at temperatures T_h and T_c, respectively.

The system of governing equations (8)-(11) in conjunction with the boundary conditions stated earlier is solved through a control-volume formulation of the finite-difference method. The pressure-velocity coupling is handled through the SIMPLE-C algorithm described by Van Doormaal and Raithby [41], which is essentially a more implicit variant of the SIMPLE algorithm developed by Patankar and Spalding [42], whose details are thoroughly described in [43]. The advection fluxes are evaluated by the QUICK discretization scheme proposed by [44]. The computational spatial domain is filled with a non-uniform grid, having a higher concentration of grid lines near the boundary walls, and a lower uniform spacing throughout the remainder interior of the cavity. Starting from the first-approximation fields of the dependent variables across the cavity, *i. e*. uniform dimensionless temperature set to 0 and nanofluid at rest, the discretized system of algebraic governing equations is solved iteratively by way of a line-by-line application of the Thomas algorithm. A standard under-relaxation technique is enforced in all steps of the computational procedure to ensure adequate convergence. The numerical solution of the velocity and temperature fields is considered to be converged when the maximum absolute values of the mass source, as well as the percentage changes of the dependent variables at any grid-node between two consecutive iterations, are smaller than the pre-specified values, *i. e*. 10^{-4} and 10^{-6}, respectively. In addition, the further condition that the relative difference between the incoming and outgoing heat transfer rates at the heated and cooled sidewalls is smaller than the pre-assigned value of 10^{-4}, must be verified.

After convergence of the velocity and temperature fields is satisfactorily attained, the effective local Nusselt numbers $(\mathrm{Nu}_Y)_\mathrm{h}$ for the heated sidewall and $(\mathrm{Nu}_Y)_\mathrm{c}$ for the cooled sidewall are calculated with the expressions:

$$(\mathrm{Nu}_Y)_\mathrm{h} = \frac{(h_Y)_\mathrm{h} W}{k_\mathrm{h}} = \frac{q_\mathrm{h} W}{k_\mathrm{h}(T_\mathrm{h} - T_\mathrm{c})} = -\left.\frac{\partial\theta}{\partial X}\right|_{X=0} \tag{21}$$

$$(\mathrm{Nu}_Y)_\mathrm{c} = \frac{(h_Y)_\mathrm{c} W}{k_\mathrm{c}} = \frac{q_\mathrm{c} W}{k_\mathrm{c}(T_\mathrm{c} - T_\mathrm{h})} = -\left.\frac{\partial\theta}{\partial X}\right|_{X=1} \tag{22}$$

where $(h_Y)_\mathrm{h}$ and $(h_Y)_\mathrm{c}$ are the local coefficients of convection at the heated and cooled sidewalls, respectively, q_h and q_c – the heat fluxes at the heated and cooled sidewalls, respectively, and k_h and k_c – the values of the effective thermal conductivity calculated at temperatures T_h and T_c, respectively. The temperature gradients in eqs. (21) and (22) are evaluated by a second-order temperature profile embracing the wall-node and the two adjacent fluid-nodes. Similarly, the corresponding pair of effective average Nusselt numbers Nu_h and Nu_c are:

$$\mathrm{Nu}_\mathrm{h} = \frac{h_\mathrm{h} W}{k_\mathrm{h}} = \frac{Q_\mathrm{h}}{k_\mathrm{h}\left(T_\mathrm{h} - T_\mathrm{c}\right)} = -\int_0^1 \left.\frac{\partial\theta}{\partial X}\right|_{X=0} \mathrm{d}Y \tag{23}$$

$$\mathrm{Nu}_\mathrm{c} = \frac{h_\mathrm{c} W}{k_\mathrm{c}} = \frac{Q_c}{k_\mathrm{c}(T_\mathrm{c} - T_\mathrm{h})} = -\int_0^1 \left.\frac{\partial\theta}{\partial X}\right|_{X=1} \mathrm{d}Y \tag{24}$$

where h_h and h_c are the average coefficients of convection at the heated and cooled sidewalls, respectively, and Q_h and Q_c – the heat transfer rates per unit length added to the nanofluid by the heated sidewall and withdrawn from the nanofluid by the cooled sidewall, respectively. As far as the integrals appearing in eqs. (23) and (24) are concerned, they are computed numerically by means of the trapezoidal rule.

Because at steady-state the incoming and outgoing heat transfer rates per unit length are the same, *i. e*. $Q_\mathrm{h} = -Q_\mathrm{c} = Q$, the relationship between Nu_h and Nu_c holds:

$$\mathrm{Nu}_\mathrm{h}\, k_\mathrm{h} = \mathrm{Nu}_\mathrm{c}\, k_\mathrm{c} \tag{25}$$

Numerical tests related to the dependence of the results on the mesh-spacing have been methodically performed for several combinations of the five controlling parameters, namely Ra_f, d_p, φ, T_c, and T_h. The optimal grid-size values, *i. e.* those used for computations, are such that further refinements do not produce noticeable modifications either in the heat transfer rates or in the flow field. Specifically, the percentage changes of Nu_h and Nu_c, and those of the maximum velocity components U_max and V_max on the vertical and horizontal midplanes of the enclosure, are smaller than the pre-established accuracy value, *i. e.*, 1%. The typical number of nodal points used for computations lies in the ranges between 40 × 40 and 120 × 120. Selected results of the grid sensitivity analysis are presented in tab. 1, in which the values of Nu_h, Nu_c, U_max, and V_max, and their respective percent changes between consecutive mesh sizes, are reported for T_c = 303 K, and T_h = 313 K. It may be seen that a denser grid is required at higher Rayleigh numbers (note that a mesh size of 50 × 50 is deemed to be adequate at $\mathrm{Ra}_\mathrm{f} = 10^4$, φ = 0.01, and d_p = 25 nm, whilst a mesh size of 100 × 100 is necessitated at $\mathrm{Ra}_\mathrm{f} = 10^6$, φ = 0.01, and d_p = 25 nm). In contrast, the grid-spacing is practically insensitive to the con-

Table 1. Grid sensitivity analysis for T_c = 303 K and T_h = 313 K

Ra_f	φ	d_p [nm]	Mesh size	Nu_h	%	Nu_c	%	U_max	%	V_max	%
10^4	0.01	25	20 × 20	2.210		2.321		2.96		3.50	
			30 × 30	2.179	–1.41	2.288	–1.42	2.97	+0.45	3.59	+2.46
			40 × 40	2.167	–0.55	2.275	–0.58	2.985	+0.51	3.620	+0.94
			50 × 50	2.161	–0.25	2.270	–0.25	2.988	+0.12	3.628	+0.22
			60 × 60	2.158	–0.17	2.266	–0.17	2.989	+0.00	3.629	+0.02
			80 × 80	2.154	–0.17	2.262	–0.17	2.985	–0.10	3.630	+0.02
			100 × 100	2.141	–0.60	2.249	–0.58	2.985	+0.00	3.631	+0.03
10^6	0.01	25	40 × 40	9.400		9.872		15.303		40.648	
			50 × 50	9.180	–2.34	9.641	–2.34	15.146	–1.03	42.528	+4.62
			60 × 60	9.057	–1.34	9.511	–1.35	15.066	–0.53	41.995	–1.25
			80 × 80	8.932	–1.38	9.380	–1.37	14.975	–0.61	42.950	+2.27
			100 × 100	8.873	–0.66	9.318	–0.66	14.922	–0.35	43.192	+0.56
10^6	0.04	25	40 × 40	7.918		8.576		10.855		27.795	
			50 × 50	7.769	–1.89	8.414	–1.89	10.758	–0.89	27.937	+0.51
			60 × 60	7.687	–1.06	8.325	–1.06	10.695	–0.59	28.187	+0.90
			80 × 80	7.603	–1.08	8.235	–1.09	10.627	–0.64	28.334	+0.52
			100 × 100	7.564	–0.52	8.192	–0.51	10.613	–0.13	28.405	+0.25
10^6	0.04	100	40 × 40	8.646		9.168		13.170		34.475	
			50 × 50	8.464	–2.10	8.975	–2.11	13.054	–0.88	35.315	+2.44
			60 × 60	8.363	–1.20	8.867	–1.19	12.980	–0.57	35.022	–0.83
			80 × 80	8.261	–1.22	8.759	–1.22	12.894	–0.66	35.461	+1.25
			100 × 100	8.213	–0.58	8.709	–0.58	12.844	–0.39	35.816	+1.00

centration of the suspended nanoparticles (at $Ra_f = 10^6$ and $d_p = 25$ nm the same mesh size of 100 × 100 gives acceptable results for both volume fractions $\varphi = 0.01$ and $\varphi = 0.04$), as well as to the nanoparticle size (at $Ra_f = 10^6$ and $\varphi = 0.04$ the 100 × 100 mesh size is adequate for both diameters $d_p = 25$ nm and $d_p = 100$ nm). Moreover, some test runs have also been executed with the first-approximation uniform value of θ set to 0.5 or 1, rather than 0, with the aim to determine what effect these starting conditions could have on the flow and temperature patterns. Solutions practically identical to those obtained assuming $\theta = 0$ throughout the enclosure were obtained for all the configurations examined. Finally, with the scope to validate the numerical code used for the present study, the solutions obtained for a differentially heated square cavity filled with air, whose physical properties were assumed to be constant, have been compared with the benchmark results derived by de Vahl Davis [45] through a standard finite-difference method, as shown in tab. 2.

Table 2. Comparison of the present solutions with the benchmark solutions of de Vahl Davis (BM1), Mahdi and Kinney + Hortman *et al.* (BM2), Wan *et al.* by FEM (BM3), and Wan *et al.* by DSC (BM4) for a differentially heated square cavity at steady-state

Quantities	Present work	BM1	BM2	BM3	BM4
$Ra = 10^3$					
U_{max}	3.654	3.649	3.649	3.489	3.643
V_{max}	3.708	3.697	3.690	3.686	3.686
Nu	1.116	1.118	1.113	1.117	1.073
$Ra = 10^4$					
U_{max}	16.242	16.178	16.180	16.122	15.967
V_{max}	19.714	19.617	19.629	19.790	19.980
Nu	2.254	2.243	2.244	2.254	2.155
$Ra = 10^5$					
U_{max}	35.008	34.730	34.739	33.390	33.510
V_{max}	68.109	68.590	68.639	70.630	70.810
Nu	4.506	4.519	4.521	4.598	4.352
$Ra = 10^6$					
U_{max}	65.226	64.630	64.836	65.400	65.550
V_{max}	221.598	219.360	220.461	227.110	227.240
Nu	8.879	8.800	8.825	8.976	8.632

It may be seen that the average Nusselt numbers as well as the maximum horizontal and vertical velocity components, on the vertical and horizontal midplanes of the enclosure, respectively, are well within 1% of the benchmark data listed in column BM1. The following additional benchmark solutions are also reported for further comparison:

- the results obtained through finite-volume methods by Mahdi and Kinney [46], for $Ra = 10^3$, and by Hortman *et al.* [47], for $Ra = 10^4$–10^6, are listed in column BM2,
- the results obtained through a finite-element method by Wan *et al.* [48] are listed in column BM3, and
- the results obtained through a discrete singular convolution algorithm by Wan *et al.* [48] are listed in column BM4.

It is worth noticing that our dimensionless velocity results have been multiplied by the Prandtl number before being inserted in tab. 2, so as to account for the choice of the ratio between kinematic viscosity of the fluid and characteristic length as scale factor for the velocity, instead of the ratio between thermal diffusivity of the fluid and characteristic length used in [45-48]. In addition, the values of the average Nusselt number computed numerically under the assumption of constant physical properties for Pr = 7 (which corresponds to water) and

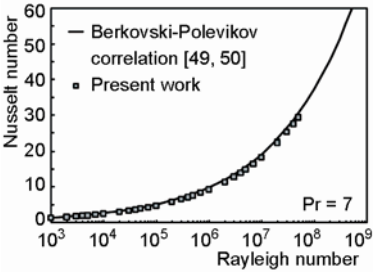

Figure 2. Comparison between the present numerical results and the Berkovsky-Polevikov correlation for a water-filled square enclosure differentially heated at sides

Rayleigh numbers in the range 10^3-$5\cdot10^7$ have been compared with the usually recommended Berkovsky-Polevikov correlation based on experimental and numerical data of laminar natural convection in a rectangular cavity heated and cooled from the side with an aspect ratio near unity, *e. g.* [49] and [50]. The comparative analysis, displayed in fig. 2, demonstrates that the correspondence between numerical results and literature data is widely satisfactory.

Results and discussion

Numerical simulations are performed for different values of:

– the nanoparticle volume fraction, φ, in the range between 0 and 0.06,
– the diameter of the suspended nanoparticles, d_p, in the range between 25 nm and 100 nm,
– the temperature of the cooled sidewall, T_c, in the range between 293 K and 313 K,
– the temperature of the heated sidewall, T_h, in the range between 298 K and 343 K (correspondingly, the temperature difference between the sidewalls, $\Delta T = T_h - T_c$, spans from 5 K to 50 K), and
– the Rayleigh number of the base fluid, Ra_f, in the range between 10^3 and 10^7.

Notice that, once the value of T_c is assigned, either the temperature difference between the sidewalls, ΔT, or the nanofluid average temperature, $T_{av} = (T_h + T_c)/2$, may be taken as an independent variable instead of T_h.

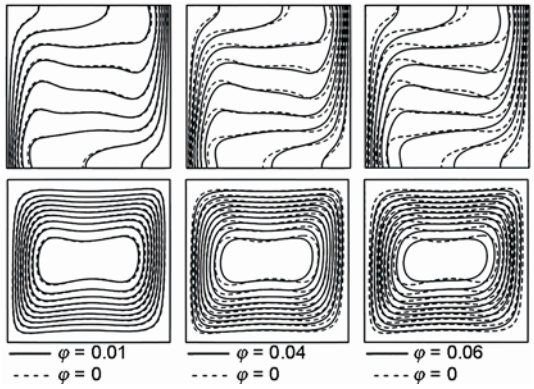

Figure 3. Effect of the nanoparticle volume fraction on the isotherm and streamline contour plots for $Ra_f = 10^5$, $T_c = 303$ K, $\Delta T = 10$ K, and $d_p = 25$ nm, at $\varphi = 0.01$ (left), $\varphi = 0.04$ (middle), and $\varphi = 0.06$ (right); dashed line plots refer to pure fluid

A selection of local results is presented in figs. 3-7, in which the isotherm and streamline contours are plotted for different sets of values of φ, d_p, T_c, T_h, and Ra_f, in order to highlight the effects of these independent variables on the temperature and velocity fields. The contour lines of the isotherm plots correspond to equally-spaced values of the dimensionless temperature θ in the range between 0 and 1. The contour lines of the streamline plots correspond to equally-spaced absolute values of the normalized dimensionless stream function $\Psi/|\Psi|_{max}$ in the range between 0 and 1, where Ψ is defined by relations:

$$\rho^* U = \frac{\partial \Psi}{\partial Y}, \quad \rho^* V = -\frac{\partial \Psi}{\partial X} \tag{26}$$

As expected, for all the configurations examined the flow field consists of a single roll-cell that derives from the rising of the hot fluid adjacent to the heated sidewall and its descent along the opposite cooled sidewall. It may be observed that when φ increases and d_p decreases, figs. 3 and 4, the consequent growth of μ entails a decrease in the motion intensity, as reflected by the expansion of the streamlines toward the core of the cavity. Typical profiles of

the velocity components U and V along the vertical and horizontal midplanes of the enclosure, respectively, are displayed in fig. 8 for d_p = 25 nm, T_c = 303 K, T_h = 313 K, and $Ra_f = 10^5$, with φ as a parameter. Correspondingly, the isotherm lines tend to be less compressed toward the heated and cooled sidewalls of the enclosure. However, since at same time also k increases, the decrease of the local temperature gradients at both sidewalls does not necessarily imply a degradation of the local heat transfer. This is clearly shown in fig. 9, where a set of typical distributions of the effective local Nusselt number along the heated sidewall $(Nu_Y)_h$, and the corresponding distributions of the local coefficient of convection $(h_Y)_h = (Nu_Y)_h k_h/W$, are displayed for the same values of φ, d_p, T_c, T_h, and Ra_f previously used in fig. 8. It may be seen that, fixed d_p = 25 nm, T_c = 303 K, T_h = 313 K, and $Ra_f = 10^5$, the amount of heat exchanged at φ = 0.01 is higher than that transferred across the pure base fluid. *Vice versa*, at φ = 0.04 and 0.06 the heat transfer rate is lower, which means that the diminution of the temperature gradients at the sidewalls prevails on the increase of the effective thermal conductivity.

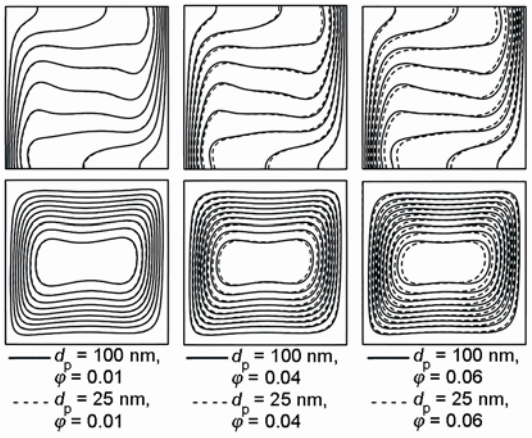

Figure 4. Effect of the nanoparticle diameter on the isotherm and streamline contour plots for $Ra_f = 10^5$, T_c = 303 K, ΔT = 10 K, and d_p = 25 nm (dashed line plots), and 100 nm (continuous line plots), at φ = 0.01 (left), φ = 0.04 (middle), and φ = 0.06 (right)

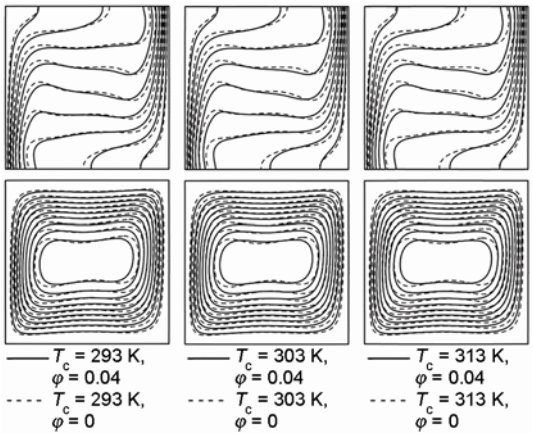

Figure 5. Effect of the temperature of the cooled wall on the isotherm and streamline contour plots for $Ra_f = 10^5$, φ = 0.04, ΔT = 10 K, and d_p = 25 nm, with T_c = 293 K (left), T_c = 303 K (middle), and T_c = 313 K (right); dashed lines plots refer to pure fluid

As far as the effects of temperatures T_c and T_h are concerned, figs. 5 and 6, the thermal field is affected much more by the increase of ΔT for a fixed value of T_c, than by the increase of T_c (or T_h) for a fixed value of ΔT, as denoted by the progressively more pronounced deformation of the isotherms that occurs as ΔT is magnified. In fact, fixed T_c, the degree of compression of the isotherm lines toward the heated sidewall must decrease with increasing ΔT so as to ensure that the heat transfer rates at both sides of the enclosure are the same. Regarding the effects of T_c and T_h on the velocity field, the motion intensity increases as T_c and/or T_h are increased, which is due to the fact that μ decreases with increasing T (following the same law of the pure base liquid).

Moreover, the degree of deformation of both the velocity and temperature fields with respect to the case of pure base liquid is practically insensitive to the Rayleigh number of the base fluid, at least for relatively high Rayleigh numbers, *i. e.* $Ra_f > 10^5$, fig. 7. Conversely, for $Ra_f \le 10^5$ a decrease in the Rayleigh number leads to a reduction of the local temperature

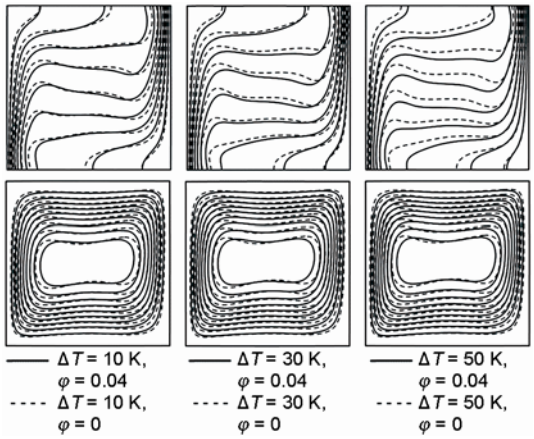

Figure 6. Effect of the sidewall temperature difference on the isotherm and streamline contour plots for Ra_f = 105, φ = 0.04, T_c = 293 K, and d_p = 25 nm, with ΔT = 10 K (left), ΔT = 30 K (middle), and ΔT = 50 K (right); dashed line plots refer to pure fluid

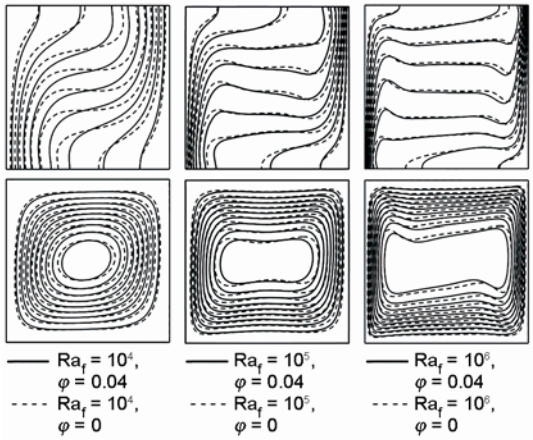

Figure 7. Effect of the base-fluid Rayleigh number on the isotherm and streamline contour plots in $Al_2O_3 + H_2O$ for φ = 0.04, T_c = 303 K, ΔT = 10 K, and d_p = 25 nm, at $Ra_f = 10^4$ (left), $Ra_f = 10^5$ (middle), and $Ra_f = 10^6$ (right); dashed line plots refers to pure fluid

gradients and a less accentuated fluid stratification in the middle of the cavity. This could be imputed to the fact that the effect of the velocity diminution produced by the addition of solid nanoparticles to the base liquid (consequent to increase of μ) is percentually more remarkable when the fluid motion intensity is low, *i. e.* at small Rayleigh numbers, at which a conduction-dominated regime may tend to establish.

Finally, a comparison between the solutions obtained in the present study and the local fields that would have been derived by adopting the conventional Maxwell-Garnett and Brinkman models for the calculation of k and μ, in conjunction with the common assumption of constant physical properties, is presented in fig. 10, showing the failure of the simulation procedures based on the traditional mean-field theories. On the other hand, owing to the significant increase of k with T, the hypothesis of constant physical properties should be avoided, at least when ΔT is higher than 10 K.

As far as the overall results are concerned, the increased heat transfer performance consequent to the dispersion of nanoparticles into the base liquid is expressed in terms of the heat transfer enhancement, E, defined as:

$$E = \frac{h_{\mathrm{h}}}{(h_{\mathrm{f}})_{\mathrm{h}}} - 1 = \frac{\mathrm{Nu}_{\mathrm{h}}}{(\mathrm{Nu}_{\mathrm{f}})_{\mathrm{h}}}\left(\frac{k}{k_{\mathrm{f}}}\right)_{\mathrm{h}} - 1 \quad (27)$$

where $(h_f)_h$ and $(Nu_f)_h$ are the coefficient of convection and the average Nusselt number at the heated sidewall for the pure base liquid, h_h and Nu_h – the corresponding effective quantities of the nanoparticle suspension, and $(k/k_f)_h$ is the value of the thermal conductivity ratio calculated at temperature T_h. Obviously, according to eq. (25), the same value of E can be obtained by replacing subscript "*h*" with "*c*" in eq. (27), that corresponds to make reference to the cooled sidewall rather than to the heated sidewall for the computation of the heat transfer enhancement.

The effects of the nanoparticle size, the buoyancy strength and the nanofluid temperature on the heat transfer performance of the enclosure are displayed in figs. 11-13. It is apparent that, owing to the dispersion of a progressively larger amount of solid nanoparticles

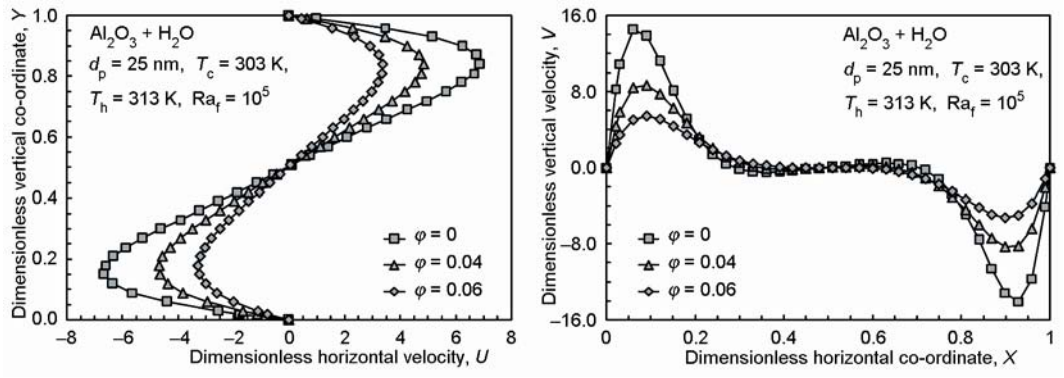

Figure 8. Distributions of *U vs. Y* along the vertical midplane with φ as a parameter (left) and *V vs. X* along the horizontal midplane with φ as a parameter (right)

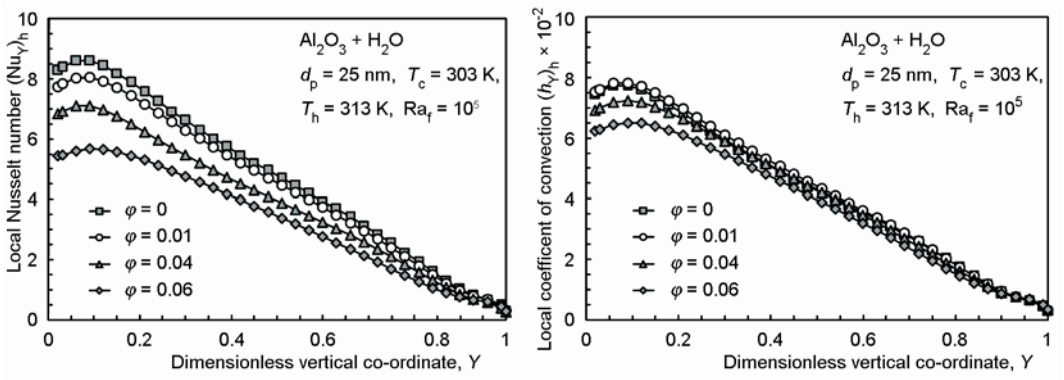

Figure 9. Distributions of the local effective Nusselt number $(Nu_Y)_h$ *vs. Y* with φ as a parameter (left) and the local coefficient of convection $(h_Y)_h$ *vs. Y* with φ as a parameter (right)

into the base liquid, the heat transfer enhancement increases up to a point, which is due to the increased effective thermal conductivity. The value of φ corresponding to the peak of E is defined as the optimal particle loading for maximum heat transfer enhancement, denoted as φ_{opt}. As the volume fraction is further increased above φ_{opt}, the heat transfer enhancement decreases, which is due to the excessive growth of the effective viscosity. Obviously, when the increased viscosity effect outweighs the increased thermal conductivity effect, the heat transfer enhancement becomes negative, which means that the use of the nanofluid brings to a deterioration in the convective heat transfer performance. Notice that both E and φ_{opt} increase as d_p is decreased and T_{av} is increased, which is in full agreement with the theoretical data previously reported and discussed in [28]. Additionally, E increases as Ra_f is increased (although such an increase is quite moderate and

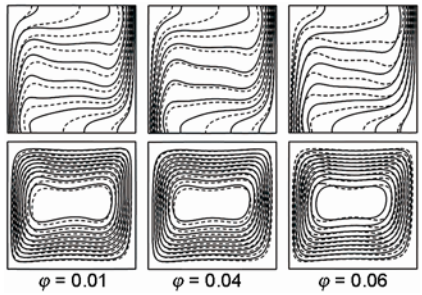

Figure 10. Comparison between the results of the present study (continuous lines) and a constant-properties study using the Maxwell-Garnett model and Brinkman equation (dashed lines) in $Al_2O_3 + H_2O$ for $Ra_f = 10^5$, T_c = 293 K, ΔT = 50 K, and d_p = 25 nm, at φ = 0.01-0.06

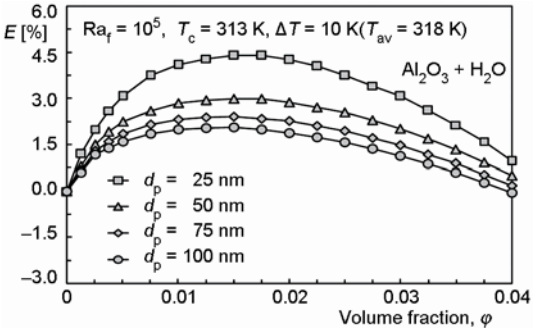

Figure 11. Distributions of E [%] *vs.* φ with d_p as a parameter

tends to vanish at high Rayleigh numbers), whilst φ_{opt} is practically independent of Ra_f. Regarding the temperature effects, the comparison of the diagrams shown in fig. 13 points out that, for any assigned value of T_{av}, the heat transfer enhancement is much more sensitive to increases in ΔT for a fixed value of T_c, rather than increases in T_c for a fixed value of ΔT (on the other hand, also the local fields are affected much more by the value of ΔT than by the value of T_c, as discussed earlier). Another peculiarity is that the temperature-dependence of φ_{opt} can be expressed simply in terms of T_{av}, at least as long as ΔT does not exceed 30 K. In this connection, the same dimensional algebraic equation proposed in [28] can be used to evaluate the percentage optimal particle loading with a 2.95% standard deviation of error:

$$\varphi_{opt}(\%) = (5\cdot 10^{-4})\,[t_{av}(°C)]^{2.335}[d_p(nm)]^{-0.19} \qquad 5\ \text{K} \le \Delta T \le 30\ \text{K, and } 10^4 \le \text{Ra}_f \le 10^7 \quad (28)$$

where t_{av} (°C) is the average temperature of the nanofluid expressed in degrees Celsius, and d_p (nm) is the nanoparticle diameter in nm.

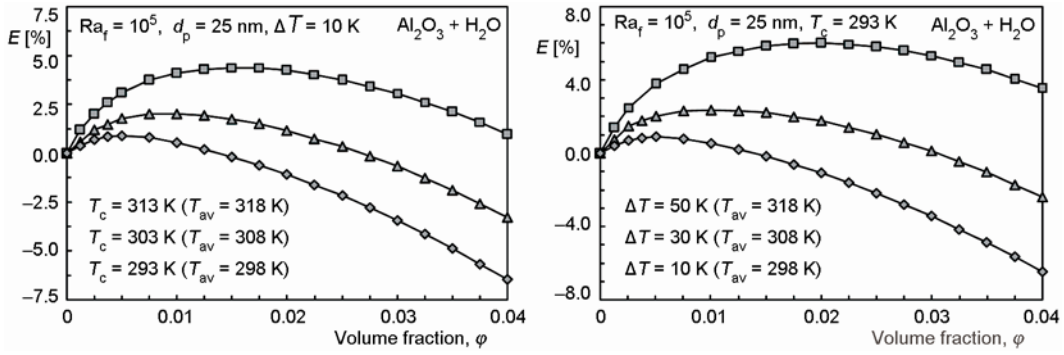

Figure 12. Distributions of E [%] *vs.* φ with T_c as a parameter (left) or ΔT as a parameter (right)

Finally, a semi-empirical correlation is developed for predicting the effective average Nusselt number of the cooled sidewall, Nu_c defined in eq. (25), as a function of the effective Rayleigh and Prandtl numbers, and the temperatures of the heated and cooled sidewalls, T_h and T_c:

$$\text{Nu}_c = \left[0.34\left(\frac{\text{Pr}}{0.326+\text{Pr}}\text{Ra}\right)^{0.27}\left(\frac{T_h - T_c}{T_c}\right)^{0.087}\right] - 0.6 \quad (29)$$

The percent standard deviation of error and the percent range of error of eq. (29) are 1.12% and ±3.9%, respectively (fig. 14). Notice that eq. (29) is valid for 293 K ≤ T_c ≤ 313 K, 298 K ≤ T_h ≤ 343 K, and $10^4 \le \text{Ra}_f \le 10^7$. Recall that Ra and Pr, defined in eq. (12), can be expressed in terms of Ra_f and Pr_f, respectively, through the relations given in eq. (20), and that the effective properties appearing in Ra and Pr must be calculated at the reference temperature

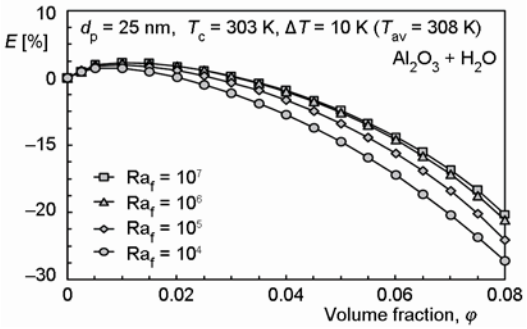

Figure 13. Distributions of E [%] *vs.* φ with Ra_f as a parameter

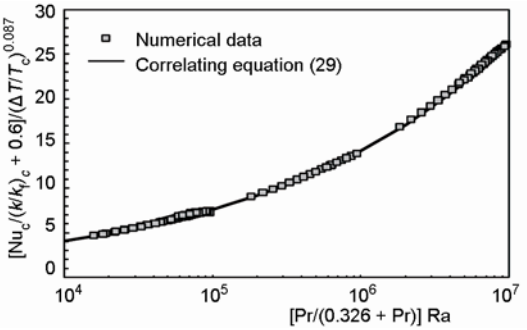

Figure 14. Comparison between eq. (29) and the numerical data of Nu

$T_r = T_c$. Once Nu_c is known from eq. (29), the value of the effective average Nusselt number of the heated sidewall of the enclosure, Nu_h, can be calculated through eq. (25).

Conclusions

Laminar natural convection of $Al_2O_3 + H_2O$ nanofluids inside a square cavity differentially heated at sides has been studied numerically. Assuming that the nanofluid behaves like a single-phase fluid, the system of the mass, momentum, and energy transfer governing equations, in which the thermophysical properties are the nanofluid effective properties, has been solved by a computational code based on the SIMPLE-C algorithm. The nanofluid has been assumed to be Newtonian with temperature-dependent effective properties. The effective thermal conductivity and dynamic viscosity have been estimated through a pair of empirical equations based on a wide variety of experimental data reported in the literature. The other effective physical properties have been calculated by the conventional mixing theory. Simulations have been performed for different values of the temperature of the cooled sidewall in the range 293-313 K, the temperature of the heated sidewall in the range 298-343 K, the Rayleigh number of the base fluid in the range 10^3-10^7, the nanoparticle average diameter in the range 25-100 nm, and the nanoparticle volume fraction in the range 0-0.06.

The main results obtained in the present study may be summarized:

- The heat transfer enhancement consequent to the dispersion of solid nanoparticles into the base liquid increases with increasing the nanoparticle volume fraction up to an optimal particle loading at which the amount of heat transferred across the enclosure has a peak.
- The optimal particle loading increases as the diameter of the suspended nanoparticle decreases.
- The optimal particle loading increases as the nanofluid average temperature increases, much more if the temperature increase is obtained by increasing the temperature difference between the sidewalls, rather than increasing the temperatures of both sidewalls keeping unaltered their temperature difference.
- The optimal particle loading is practically independent of the Rayleigh number.

Nomenclature

c – effective specific heat at constant pressure, [$Jkg^{-1}K^{-1}$]
c_f – specific heat at constant pressure of the base fluid, [$Jkg^{-1}K^{-1}$]
c_s – specific heat at constant pressure of the solid nanoparticles, [$Jkg^{-1}K^{-1}$]
c^* – dimensionless effective specific heat at constant pressure, [–]

d_f – equivalent diameter of a base fluid molecule, [m]
d_p – nanoparticle diameter, [m]
E – heat transfer enhancement, [–]
g – gravitational acceleration, [ms^{-2}]
h – coefficient of convection of the nanofluid, [Wm^{-2}K^{-1}]
h_f – coefficient of convection of the base fluid, [Wm^{-2}K^{-1}]
h_Y – local coefficient of convection of the nanofluid, [Wm^{-2}K^{-1}]
k – effective thermal conductivity, [Wm^{-1}K^{-1}]
k_b – Boltzmann constant = 1.38066·10^{-23}, [JK^{-1}]
k_f – base fluid thermal conductivity, [Wm^{-1}K^{-1}]
k_s – thermal conductivity of the solid nanoparticles, [Wm^{-1}K^{-1}]
k^* – dimensionless effective thermal conductivity, [–]
M – molar mass of the base fluid, [kgmol^{-1}]
N – Avogadro number = 6.022·10^{23}, [mol^{-1}]
Nu – effective Nusselt number (= hW/k), [–]
Nu_f – Nusselt number of the base fluid (= h_f W/k$_f$), [–]
Nu_Y – local effective Nusselt number (= h_Y W/k), [–]
P – dimensionless pressure, [–]
p – pressure, [Pa]
Pr – effective Prandtl number (= $c\mu/k$), [–]
Pr_f – Prandtl number of the base fluid (= $c_f\mu_f/k_f$), [–]
Q_c – heat transfer rate per unit length withdrawn from the nanofluid by the cooled sidewall, [Wm^{-1}]
Q_h – heat transfer rate per unit length added to the nanofluid by the heated sidewall, [Wm^{-1}]
q_c – heat flux at the cooled sidewall, [Wm^{-2}]
q_h – heat flux at the heated sidewall, [Wm^{-2}]
Ra – effective Rayleigh number (= $\rho c g\Delta\rho$ W^3/kμ), [–]
Ra_f – Rayleigh number of the base fluid (= $\rho_f c_f g\Delta\rho_f$ W^3/k$_f\mu_f$), [–]
Re – nanoparticle Reynolds number (= $2\rho_f k_b T/\pi\mu_f^2 d_p$), [–]
T – temperature, [K]
T_{av} – average temperature of the enclosed fluid, [K]
T_c – temperature of the cooled sidewall of the enclosure, [K]
T_{fr} – freezing point of the base liquid, [K]
T_h – temperature of the heated sidewall of the enclosure, [K]
U – dimensionless horizontal velocity component, [–]
u – horizontal velocity component, [ms^{-1}]
V – dimensionless vertical velocity component, [–]
v – vertical velocity component, [ms^{-1}]
W – width of the enclosure, [m]
X – dimensionless horizontal Cartesian co-ordinate, [–]
x – horizontal Cartesian co-ordinate, [m]
Y – dimensionless vertical Cartesian co-ordinate, [–]
y – vertical Cartesian co-ordinate, [m]

Greek symbols

θ – dimensionless temperature, [–]
μ – effective dynamic viscosity, [kgm^{-1}s^{-1}]
μ_f – dynamic viscosity of the base fluid, [kgm^{-1}s^{-1}]
μ^* – dimensionless effective dynamic viscosity, [–]
ρ – effective mass density, [kgm^{-3}]
ρ_f – mass density of the base fluid, [kgm^{-3}]
ρ_s – mass density of the solid nanoparticles, [kgm^{-3}]
ρ^* – dimensionless effective mass density, [–]
φ – nanoparticle volume fraction, [–]
Ψ – dimensionless stream function, [–]

Subscripts

c – at the temperature of the cooled sidewall of the enclosure
f – base fluid
h – at the temperature of the heated sidewall of the enclosure
max – maximum value
opt – optimal value
r – at the reference temperature
s – solid phase

References

[1] Khanafer, K., *et al*., Buoyancy-Driven Heat Transfer Enhancement in a Two-Dimensional Enclosure Utilizing Nanofluids, *Int. J. Heat Mass Transfer*, *46* (2003), 19, pp. 3639-3653
[2] Jou, R.-Y., Tzeng, S.-C., Numerical Research of Nature Convective Heat Transfer Enhancement Filled with Nanofluids in Rectangular Enclosures, *Int. Comm. Heat Mass Transfer*, *33* (2006), 6, pp. 727-736
[3] Oztop, H. F., Abu-Nada, E., Numerical Study of Natural Convection in Partially Heated Rectangular Enclosures Filled with Nanofluids, *Int. J. Heat Fluid Flow*, *29* (2008), 5, pp. 1326-1336
[4] Abu-Nada, E., Oztop, H. F., Effects of Inclination Angle on Natural Convection in Enclosures Filled with Cu-Water Nanofluid, *Int. J. Heat Fluid Flow*, *30* (2009), 4, pp. 669-678

[5] Kahveci, K., Buoyancy Driven Heat Transfer of Nanofluids in a Tilted Enclosure, *J. Heat Transfer*, *132* (2010), 062501
[6] Kefayati, G. H. R., *et al*., Lattice Boltzmann Simulation of Natural Convection in Tall Enclosures Using Water/SiO_2 Nanofluid, *Int. Comm. Heat Mass Transfer*, *38* (2011), 6, pp. 798-805
[7] Lai, F.-H., Yang, Y.-T., Lattice Boltzmann Simulation of Natural Convection Heat Transfer of Al_2O_3/Water Nanofluids in a Square Enclosure, *Int. J. Thermal Sciences*, *50* (2011), 10, pp. 1930-1941
[8] Abu-Nada, E., *et al*., Effects of Nanofluid Variable Properties on Natural Convection in Enclosures, *Int. J. Thermal Sciences*, *49* (2010), 3, pp. 479-491
[9] Lin, K. C., Violi A., Natural Convection Heat Transfer of Nanofluids in a Vertical Cavity: Effects of non-Uniform Particle Diameter and Temperature on Thermal Conductivity, *Int. J. Heat Fluid Flow*, *31* (2010), 2, pp. 236-245
[10] Abu-Nada E., Chamkha A. J., Effect of Nanofluid Variable Properties on Natural Convection in Enclosures Filled with a CuO-EG-Water Nanofluid, *Int. J. Thermal Sciences*, *49* (2010), 12, pp. 2339-2352
[11] Maxwell-Garnett, J. C., *A Treatise on Electricity and Magnetism*, 3rd ed., Dover, New York, USA, 1954
[12] Brinkman, H. C., The Viscosity of Concentrated Suspensions and Solutions, *J. Chem. Phys.*, *20* (1952), 4, pp. 571
[13] Hamilton, R. L., Crosser, O. K., Thermal Conductivity of Heterogeneous Two Component Systems, *Ind. Eng. Chem. Fundam.*, *1* (1962), 3, pp. 187-191
[14] Bruggemann, D. A. G., Calculation of Effective Constitutive Parameters of Heterogeneous Substances, I, Permittivity and Conductivity for Dilute Composite Mediums of Isotropic Substances (in German), *Ann. Phys.*, *24* (1935), pp. 636-679
[15] Eapen, J., *et al.*, Mean-Field Versus Microconvection Effects in Nanofluid Thermal Conduction, *Phys. Rev. Lett.*, *99* (2007), 095901
[16] Buongiorno, J., *et al.*, A Benchmark Study on the Thermal Conductivity of Nanofluids, *J. Appl. Phys.*, *106* (200), 094319
[17] Das, S. K., *et al*., Temperature Dependence of Thermal Conductivity Enhancement for Nanofluids, *J. Heat Transfer*, *125* (2003), 4, pp. 567-574
[18] Li, C. H., Peterson, G. P., Experimental Investigation of Temperature and Volume Fraction Variations on the Effective Thermal Conductivity of Nanoparticle Suspensions (Nanofluids), *J. Appl. Phys.*, *99* (2006), 084314
[19] Yu, W., *et al*., Investigation on the Thermal Transport Properties of Ethylene Glycol-Based Nanofluids Containing Copper Nanoparticles, *Powder Tecnology*, *197* (2010), 3, pp. 218-221
[20] Chen, H., *et al*., Rheological Behaviour of Nanofluids, *New Journal of Physics*, *9* (2007), 10, paper No. 367
[21] Chen, H., *et al*., Rheological Behaviour of Ethylene Glycol Based Titania Nanofluids, *Chem. Phys. Lett.*, *444* (2007), 4, pp. 333-337
[22] Chevalier, J., *et al*., Rheological Properties of Nanofluids Flowing through Microchannels, *Appl. Phys. Lett.*, *91* (2007), 233103
[23] Einstein, A., A New Determination of Molecular Dimensions (in German), *Ann. Phys.*, *19* (1906), 2, pp. 289-306
[24] Einstein, A., Amendments on my Previous Work: A New Determination of Molecular Dimensions (in German), *Ann. Phys.*, *34* (1911), 3, pp. 591-592
[25] Putra, N., *et al*., Natural Convection of Nano-Fluids, *Heat Mass Transfer*, *39* (2003), 8-9, pp. 775-784
[26] Nnanna, A. G. A., Experimental Model of Temperature-Driven Nanofluid, *J. Heat Transfer*, *129* (2007), 6, pp. 697-704
[27] Ho, C. J., *et al*., Natural Convection Heat Transfer of Alumina-Water Nanofluid in Vertical Square Enclosures: An Experimental Study, *Int. J. Thermal Sciences*, *49* (2010), 8, pp. 1345-1353
[28] Corcione, M., Heat Transfer Features of Buoyancy-Driven Nanofluids inside Rectangular Enclosures Differentially Heated at the Sidewalls, *Int. J. Thermal Sciences*, *49* (2010), 9, pp. 1536-1546
[29] Chang, B. H., *et al*., Natural Convection of Microparticle Suspensions in thin Enclosures, *Int. J. Heat Mass Transfer*, *51* (2008), 5, pp. 1332-1341
[30] Williams, W., *et al*., Experimental Investigation of Turbulent Convective Heat Transfer and Pressure Loss of Alumina/Water and Zirconia/Water Nanoparticle Colloids (Nanofluids) in Horizontal Tubes, *J. Heat Transfer*, *130* (2008), 4, 042412
[31] Sommers, A. D., Yerkes, K. L., Experimental Investigation into the Convective Heat Transfer and System-Level Effects of Al_2O_3-Propanol Nanofluid, *J. Nanopart. res.*, *12* (2009), 3, pp. 1003-1014

[32] Rea, U., *et al*., Laminar Convective Heat Transfer and Viscous Pressure Loss of Alumina-Water and Zirconia-Water Nanofluids, *Int. J. Heat Mass Transfer*, *52* (2009), 7, pp. 2042-2048
[33] Das, S. K., *et al*., Pool Boiling Characteristics of Nano-Fluids, *Int. J. Heat Mass Transfer*, *46* (2003), 5, pp. 851-862
[34] Prasher, R., *et al*., Measurements of Nanofluid Viscosity and its Implications for Thermal Applications, *Appl. Phys. Lett.*, *89* (2006), 133108
[35] He, Y., *et al*., Heat Transfer and Flow Behaviour of Aqueous Suspensions of TiO_2 Nanoparticles (Nanofluids) Flowing upward through a Vertical Pipe, *Int. J. Heat Mass Transfer*, *50* (2007), 11, pp. 2272-2281
[36] Kays, W., *et al*., *Convective Heat and Mass Transfer*, 4th ed., Mc Graw- Hill Companies, Inc., New York, NY, USA, 2005
[37] Corcione, M., Empirical Correlating Equations for Predicting the Effective Thermal Conductivity and Dynamic Viscosity of Nanofluids, *Energy Conv. Manag.*, *52* (2011), 1, pp. 789-793
[38] Keblinski, P., *et al*., Mechanisms of Heat Flow in Suspensions of Nano-Sized Particles (Nanofluids), *Int. J. Heat Mass Transfer*, *45* (2002), 4, pp. 855-863
[39] Pak, B. C., Cho, Y. I., Hydrodynamic and Heat Transfer Study of Dispersed Fluids with Submicron Metallic Oxide Particles, *Exp. Heat Transfer*, *11* (1998), 2, pp. 151-170
[40] Xuan, Y., Roetzel, W., Conceptions for Heat Transfer Correlation of Nanofluids, *Int. J. Heat Mass Transfer*, *43* (2000), 19, pp. 3701-3707
[41] Van Doormaal, J. P., Raithby, G. D., Enhancements of the Simple Method for Predicting Incompressible Fluid Flows, *Num. Heat Transfer*, *7* (1984), 2, pp. 147-163
[42] Patankar, S. V., Spalding, D. B., A Calculation Procedure for Heat, Mass and Momentum Transfer in Three-Dimensional Parabolic Flows, *Int. J. Heat Mass Transfer*, *15* (1972), 10, pp. 1787-1797
[43] Patankar, S. V., *Numerical Heat Transfer and Fluid Flow*, Hemisphere Publ. Co., Washington, DC, USA, 1980.
[44] Leonard, B. P., A Stable and Accurate Convective Modelling Procedure Based on Quadratic Upstream Interpolation, *Comp. Meth. in Appl. Mech. Engng.*, *19* (1979), 1, pp. 59-78
[45] de Vahl Davis, G., Natural Convection of Air in a Square Cavity: a Bench Mark Numerical Solution, *Int. J. Num. Meth. Fluids*, *3* (1983), 3, pp. 249-264
[46] Mahdi, H. S., Kinney, R. B., Time-Dependent Natural Convection in a Square Cavity: Application of a New Finite Volume Method, *Int. J. Num. Meth. Fluids*, *11* (1990), 1, pp. 57-86
[47] Hortmann, M., *et al*., Finite Volume Multigrid Prediction of Laminar Natural Convection: Bench-Mark Solutions, *Int. J. Num. Meth. Fluids*, *11* (1990), 2, pp. 189-207
[48] Wan, D. C., *et al*., A New Benchmark Quality Solution for the Buoyancy-Driven Cavity by Discrete Singular Convolution, *Num. Heat Transfer*, *40* (2001), 3, pp. 199-228
[49] Bejan, A., *Convection Heat Transfer,* 3rd ed., John Wiley & Sons, Inc., Hoboken, N. J., USA, 2004
[50] Incropera, F. P., *et al*., *Fundamentals of Heat and Mass Transfer*, 6th ed., John Wiley & Sons, Inc., Hoboken, N. J., USA, 2007

Paper submitted: January 30, 2012
Paper revised: April 2, 2013
Paper accepted: April 5, 2013